Industrial Crops & Products 245 (2026) 123248

Contents lists available at ScienceDirect

Industrial Crops & Products

journal homepage: www.elsevier.com/locate/indcrop

Amazonian palms as underestimated crops: Elastic properties of leaflets revealed by digital image correlation combined with tensile testing

Paul Cathelineau [a,b,*], Julie Bossu [b], Damien André [c], Stéphane Corn [d], Romain Léger [d], Nicolas Le Moigne [e], Julien Engel [a,f], Romain Lehnebach [b], Louise Brousseau [a,g,*]

[a] AMAP, Univ Montpellier, IRD, CIRAD, CNRS, INRAE, Montpellier, France
[b] EcoFoG, AgroParisTech, CIRAD, CNRS, INRAE, Univ Antilles, Univ Guyane, Kourou, France
[c] Univ. Limoges, IRCER, CNRS UMR 7315, Limoges, France
[d] LMGC, Univ Montpellier, IMT Mines Alès, CNRS, Ales, France
[e] Polymers Composites and Hybrids (PCH), IMT Mines Ales, Ales, France
[f] AMAP, IRD, Herbier de Guyane, Cayenne, Guyane française, France
[g] AMAP, IRD, Cayenne, Guyane française, France

ARTICLE INFO

Keywords:
Digital Image Correlation
Tensile test
Plant materials
Biomechanics
Palms

ABSTRACT

Understanding the mechanical behaviour of plant fibres is crucial not only for advancing knowledge of plant biomechanics but also for exploring their potential in bio-based material applications. Amazonian palms, in particular, represent highly valuable but underestimated crops. Tensile tests are widely used to characterize the mechanical properties of biological materials, such as different plant organs. However, assessing their elastic properties from coupons requires accurate strain measurements, which remain challenging for such heterogeneous materials, thereby driving the development of advanced measurement techniques. This study focuses on the analysis of strain measurements using Digital Image Correlation (DIC), a non-contact optical technique that evaluates displacement fields from images captured during mechanical tests. Digital image correlation offers several advantages, including high spatial resolution, two-dimensional mapping of local strains, and non-intrusive measurement, while presenting challenges such as proper coupon positioning, image processing, accurate error quantification, and the assessment of experimental biases (e.g., offsets caused by edge curvature). This study evaluates the potential of DIC in assessing the tensile behaviour of leaflets of two Amazonian palm species (*Euterpe oleracea* and *Oenocarpus bataua)*, in comparison to laser extensometry. Repeated tensile tests allowed the estimation of the accuracy of DIC and its reliability for measuring strains, elastic moduli and Poisson's ratios. The analysis revealed significant differences in elastic moduli and Poisson's ratio between the two palm species, and spatial heterogeneity of full-field deformation within the leaflet coupons. Careful identification and exclusion of local artefacts were applied to obtain reliable measurements and ensure meaningful comparisons between the leaflets of the two studied species. Overall, these results confirm the potential of 2D-DIC for the mechanical analysis of plant materials, while also opening perspectives in understanding the relationships between anatomical structure of leaflets and their mechanical properties.

1. Introduction

Tensile tests are widely used to characterize the mechanical properties of plant materials, assessing features such as the tensile properties of tissues and cell walls (Bidhendi and Geitmann, 2018). These tests provide valuable information on key mechanical parameters, such as elastic properties (modulus of elasticity and Poisson's ratio), ultimate strength, and strain at break. These parameters can be used to hypothesize the mechanical strategies employed by plants to ensure their growth, development, and response to external stresses (e.g., wind and gravity) (Bidhendi and Geitmann, 2018). While micromechanical tools, such as piezoresistive or piezomagnetic force sensors, are well adapted to the measurement of low mechanical tensile stresses (ratio between axial loading force and area of the resistive cross-section) and are easy to implement for uniform coupons of homogeneous materials, the measurement of low strains in heterogeneous and possibly

* Corresponding authors at: AMAP, Univ Montpellier, IRD, CIRAD, CNRS, INRAE, Montpellier, France.
E-mail addresses: paul.cathelineau@ird.fr (P. Cathelineau), louise.brousseau@ird.fr (L. Brousseau).

https://doi.org/10.1016/j.indcrop.2026.123248
Received 9 October 2025; Received in revised form 4 March 2026; Accepted 10 April 2026
Available online 30 April 2026

anisotropic plant structures is much more complex.

Among the various experimental techniques for monitoring strain, crosshead displacement is rarely used due to the unreliability in strain measurement caused by slippage in the grips and frame compliance. Strain gauges, which are resistive sensors attached to the material surface, are commonly used to measure local deformations (Shah and Harle, 2017). Although they provide precise data, their application is limited to a restricted region of the material coupon, and the glue used for fixation can modify or even damage the coupon, and bias its response, and hence influence the results (Lin et al., 2024). Alternatively, mechanical extensometers, such as axial clip-ons, use displacement sensors to measure elongation between two points of the coupon. However, this method is also prone to errors due to possible slippage (Lin et al., 2024) and could damage the coupons. Another method, the uniaxial laser extensometer, offers high accuracy and a non-contact technique, but does not allow for the assessment of full-field strain, and therefore gives no information about sample anisotropy and heterogeneity (Hercher et al., 1987).

Digital image correlation (DIC) overcomes these limitations by providing non-intrusive, full-field strain measurements over the entire coupon surface with high spatial resolution. It compares high-resolution images of a coupon's surface to track the displacement of several distinct points (Passieux and Perie, 2020). Thanks to these advantages, DIC is now widely used in various scientific and engineering fields (Das et al., 2021; Dong and Pan, 2017; Haddadi and Belhabib, 2008; Khoo et al., 2016; Leclerc et al., 2010; Lecompte et al., 2006; Lin et al., 2024; Liu et al., 2025; Malowany et al., 2019; Passieux and Perie, 2020; Sánchez-Arévalo and Pulos, 2008; Seon et al., 2019; Sun et al., 2024; Zhu et al., 2024) and is also used in biomechanical studies (Alméras et al., 2024; Bao et al., 2018; Dahle, 2017; Fischer et al., 2024; Mylo and Poppinga, 2023). Despite the growing use of DIC in material sciences, its application to highly heterogeneous biological materials remains challenging due to the local mechanical heterogeneity and the presence of artefacts (out-of-plane motion and edge effects).

Palms (Arecaceae) are particularly abundant in the Amazon basin (Heijink et al., 2020; Muscarella et al., 2020; Siddiqui et al., 2024; Ter Steege et al., 2013) and are increasingly recognised as a model group for studying tropical rain forest biomes (Couvreur and Baker, 2013; Eiserhardt et al., 2011; Kissling et al., 2012; Trujillo et al., 2021). Beyond their ecological significance, palms also hold substantial cultural and economic value (Cámara-Leret et al., 2017; Coelho et al., 2021; Eiserhardt et al., 2011; Levis et al., 2017). This study focuses on two Amazonian species, *Euterpe oleracea* and *Oenocarpus bataua*, both widely used for basketry, construction, and as food (Bernal et al., 2011; Cámara-Leret et al., 2014; Granville, 1999; Kahn and Granville, 1992; Macía et al., 2011; Montúfar et al., 2010; Sosnowska and Balslev, 2009). Their use for basketry and construction is largely due to the high rigidity of their leaflets, which are composed of heterogeneous lignocellulosic tissues. Palm leaflets offer an ideal but unexplored model to evaluate the robustness and accuracy of DIC for studying the mechanical properties of heterogeneous plant tissues. Despite their high utilitarian value, Amazonian palm leaflets remain underexplored in the field of plant biomechanics. This knowledge gap limits the understanding of the relationships between their mechanical properties, and use, as well as their potential for valorisation in innovative industrial applications, such as the development of sustainable bio-based materials.

This study hypothesises that (i) DIC provides accurate and reproducible measurements of the elastic modulus, Poisson's ratio and full-field deformation of palm leaflets, and (ii) DIC is sensitive enough to detect interspecific differences in mechanical properties between morphologically distinct palm species. This work aims to demonstrate its robustness and seek to extend its applicability to the broader characterisation of plant leaf mechanical behaviour. These hypotheseses will be tackled in the two hyperdominant Amazonian palm species, *Euterpe oleracea* and *Oenocarpus bataua* (Ter Steege et al., 2013). This study addresses two current gaps (i) the lack of empirical estimates of measurement uncertainty and robustness of DIC when applied to heterogeneous plant tissues, and (ii) the scarcity of mechanical data for palm leaflets, which remain underevaluated yet potentially promising natural reinforcements.

2. Materials and methods

2.1. Leaflet sample collection and coupon preparation for tensile testing

Leaflets from three *Euterpe oleracea* (MC87_0279, MC87_0310, MC87_1027) and three *Oenocarpus bataua* palms (MC87_0074, MC87_0364, MC87_1019) were collected at the Regina site (4.0572°N, –52.0864°E) to estimate full-field systematic error and standard uncertainties obtained via DIC.

Then, leaflets were collected from 65 palms (35 *Euterpe oleracea* and 30 *Oenocarpus bataua*) at two sites – the Regina site and the Nouragues Research Station (4.0791°N, –52.6713°E) – to assess the suitability of DIC against laser extensometry and investigate interspecific variability in palm leaf biomechanics.

Living leaflets were collected from the lowest leaf in the crown (Fig. 1a). Coupons were cut along the longitudinal direction (Fig. 1b), on either side of the main vein, and cut to 100 mm in length and 10 mm in width (Fig. 1c). Coupons were stabilised for 25 h at 60°C, then in an air-conditioned room (ca. 24 °C and 60% RH) for at least two hours before testing. The thickness of the coupons was measured as the average of three measurements using a digital comparator (Mitutoyo ID-H0530, 0.0005 mm/0.001 mm).

2.2. Tensile testing with a high-resolution camera and DIC post-processing

Tensile tests based on DIC (Fig. 2a) were carried out at the Research Unit EcoFoG, Kourou, using a tensile bench (MTS 20/MH) equipped with single-grip jaws and two sensors (1 and 100 kN) coupled to a 20-megapixel resolution camera (Basler acA5472–17um).

Tests were conducted at a constant displacement speed of 1 mm/min with synchronous acquisition of image and force data at 5 Hz. A preload was set at 5 N for each test to bring the coupons to an initial stress state and ensure repeatability (Cheng et al., 2009). To avoid damaging the coupons, the tests were carried out in the elastic domain of the coupons up to a maximum load of 16 N, which was previously established by conducting tensile tests until failure on 10 coupons of *Euterpe oleracea* (See Supplementary Fig.A1). The test length on the coupon was set at 50 mm, which represents the height of the region of interest (ROI) (Fig. 2c, Fig. 3a) for the DIC algorithm. During tensile testing, strain measurements were obtained by DIC using the so-called "local" DIC technique. The principle of local DIC involves measuring a displacement field by comparing images before and during loading and then calculating strains from a discrete set of displacements by applying numerical derivation (spatial gradient). The underlying DIC algorithm employs a local approach method, analysing subsets of the reference image against the deformed image (Fig. 3b). A subset is a rectangular area within the ROI of a reference image set at the beginning with no deformation (Fig. 3a). In the proposed study, the correlation between a deformed image and the reference image is performed using the Lucas Kanade method which calculates the best possible displacement of the neighbouring pixel subset (Lucas and Kanade, 1981) by solving the optical flow equations. Here, the subset window size was set to 80 × 80 pixels, with a grid interval of 20 × 20 pixels (Fig. 3a). This configuration helps to increase the resolution of the DIC measurement by using an overlapping subset. Due to experimental and numerical biases, the resulting discrete displacement field generates systematic biases (Cheng et al., 2002; Das et al., 2021; Haddadi and Belhabib, 2008; Khoo et al., 2016; Passieux and Perie, 2020) but this has not yet been evaluated for leaflet materials. To reduce these biases, the discrete displacement field was smoothed and interpolated using a bivariate B-spline to estimate a continuous displacement field (Dierckx, 1981). The smoothed

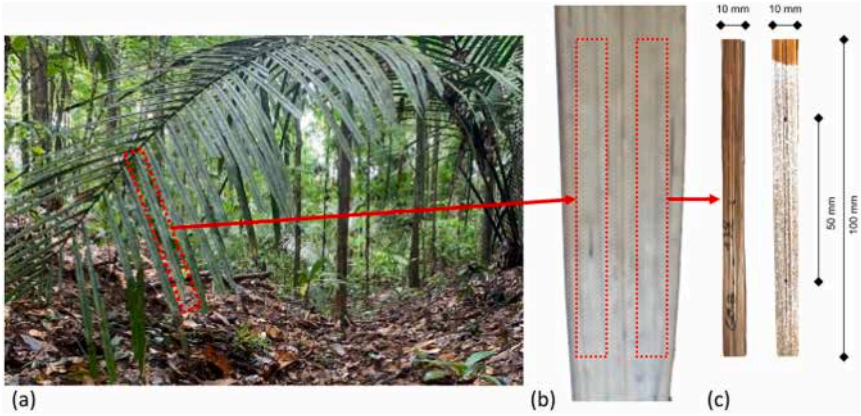

Fig. 1. Sampling and preparation of palm leaflets for tensile test: (a) example of a random selected leaflet from the lowest leaf within the crown; (b) schematic representation showing two coupons extracted on either side of the leaflet main vein and aligned with the longitudinal leaflet axis; (c) prepared coupons without and with speckle pattern (white paint), with a 100 mm in length and with two marked points spaced 50 mm, defining the Region of Interest (ROI).

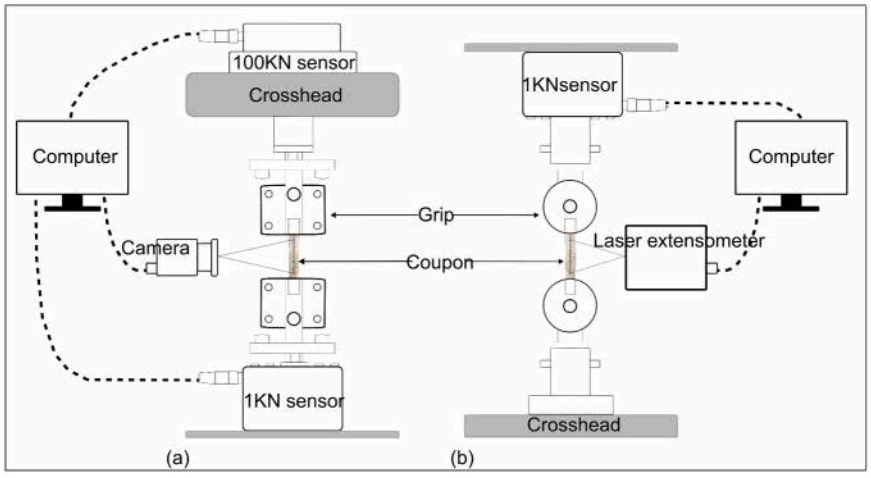

Fig. 2. Experimental setups to compare strain measurements obtained by DIC and laser extensometry: (a) tensile test using DIC: MTS 20/MH tensile bench equipped with grip and two sensors (1 and 100 kN) coupled with a camera (Basler acA5472-17um); (b) tensile test using laser extensometer: a MTS Criterion C45.105 tensile bench equipped with pneumatic grip and a 1 kN sensor coupled with a laser extensometer (LX500).

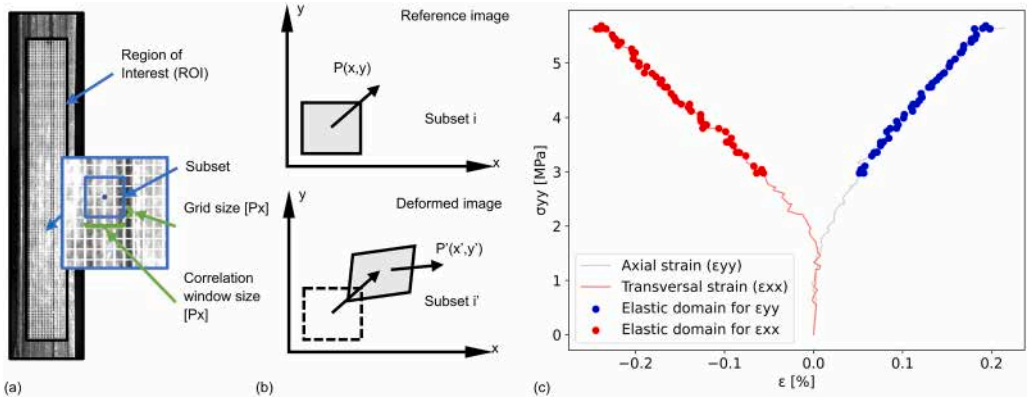

Fig. 3. Illustration of the DIC correlation process with representative stress-strain curves: (a) region of interest (ROI) on the coupon and subset used for DIC; (b) schematic representation of the reference subset to the deformed subset; (c) stress–strain curves with the elastic ε range [0.05:0.20] highlighted on ε_xx and ε_yy (colored dots).

displacement field was finally used to produce a strain field, which was calculated using second order finite strain Lagrangian tensor. The Python data-processing pipeline used in this study is based on the open-source Pydic suite (André, 2017) and adapted in order to synchronize both the force from the tensile bench and strain from the camera. Pydic is an open Python tool developed for DIC to compute displacement and strain. Pydic is based on several libraries such as Opencv, Numpy, SciPy and Matplotlib (Harris et al., 2020; Hunter,

2007; Virtanen et al., 2020). More details about the mathematical background and the related algorithms implemented in Pydic can be found in Das et al. (2021). To facilitate the DIC algorithm, coupons are often covered with a speckle in order to produce singular and randomized patterns. Stress in the axial loading direction (σ_{yy}) was calculated by dividing the force by the initial non-loaded cross-sectional area (i.e. thickness × width) of the coupon. Then, the longitudinal elastic modulus (E_y) was obtained by ordinary least squares (OLS) linear regression of the stress-strain (σ_{yy}, ε_{yy}) curves over a strain range from 0.05% to 0.2% (represented by dots on curves, Fig. 3c), to avoid any potential error measurements on ε_{xx} at the beginning and at the end of the curves. According to Hooke's law for orthotropic materials and under the assumption of uniaxial stress state, E_y can be deduced for uniaxial loading configurations with:

$$E_y = \sigma_{yy} \ / \ \varepsilon_{yy} \quad \text{Eq. 1}$$

Furthermore, Poisson's ratio (ν_{yx}), measured in the elastic domain, was determined as:

$$\nu_{yx} = - \ \varepsilon_{xx} \ / \varepsilon_{yy} \quad \text{Eq. 2}$$

where ε_{yy} corresponds to the strain in the axial loading direction, and ε_{xx} corresponds to the strain orthogonal to the axial loading direction. The same approach was applied to determine ν_{yx} by performing an OLS linear regression of $-\varepsilon_{xx}$ against ε_{yy} over the same 0.05–0.2% strain range. For each test, the force-time curve was checked to ensure there were no plateaus or sudden drops, which would indicate potential slippage or local rupture at the grips.

2.3. Evaluation of systematic error (ϵ_s) and standard uncertainties (U_A, U_B, U_C) of strain measurement using DIC

Estimation of systematic error and combined standard uncertainty of strain measurement via DIC is already well documented (Badaloni et al., 2015; Blaysat et al., 2016; Fayad et al., 2020; Iliopoulos and Andrianopoulos, 2010; Li et al., 2021; Motra et al., 2014; Su et al., 2018; Yu and Lubineau, 2019). Here, we aim to assess whether our experimental results fall within the ranges reported in previous studies. In our experiments, systematic effects (systematic error, ϵ_s, and type B standard uncertainty, U_B) are estimated from the true value of a measurand ($\varepsilon = 0$) and are attributed to the correlation algorithm implemented in the software Pydic.

The random effects (type A standard uncertainty, U_A) are estimated under repeatability conditions, which did not induce any damage to the coupons (Al-Zube et al., 2018; Al-Zube et al., 2017; Atkinson and Nevill, 1998; Nelson et al., 2019; Taylor and Kuyatt, 1994). Then, the combined standard uncertainty (U_C), which represents the repeatability, is estimated by combining systematic (type B uncertainty) and random effects (type A uncertainty).

The details of how the aforementioned errors and uncertainties were calculated are provided below:

(i) A first series of 50 images was obtained from three *Euterpe oleracea* (MC87_0279, MC87_0310, MC87_1027) and three *Oenocarpus bataua* (MC87_0074, MC87_0364, MC87_1019) coupons in the same environmental conditions (2.1–2.2). The tests were conducted without applying any force or displacement. The measurand here is the local strain (ε) at each point (node) of the ROI (Fig. 3a). For each node, the mean value (x_i^{mean}) of the displacement and strain was calculated across the images. The mean value across nodes was then compared to 0. Any deviations from 0 correspond to the systematic error (ϵ_s) of the algorithm (Haddadi and Belhabib, 2008) as follows:

$$\epsilon_s = \frac{1}{N_{nodes} N_{images}} \sum_{i=1}^{N_{nodes}} \sum_{k=1}^{Nimages} x_{i,k} \quad \text{Eq. 3}$$

where N_{images} is the number of images, N_{nodes} is the number of nodes within

the ROI and $x_{i,k}$ is the measured value for node i in image k.

The associated type B standard uncertainty (U_B) is calculated as follows:

$$U_B = \sqrt{\frac{1}{N_{nodes}} \sum_{i=1}^{N_{nodes}} (x_i^{mean} - \ \epsilon_s)^2} \quad \text{Eq. 4}$$

(ii) Then, a series of 10 repeated tensile tests was performed on the same coupons to estimate deformation and associated type A standard uncertainty (U_A). Here, the measurand is the full-field average strain measured by the DIC for a given coupon. First, the temporal and spatial average of the full-field deformation over all nodes is calculated following Eq. 3 for each repeated test. Then the result of the measurement is calculated as the mean of all repeated tests:

$$\hat{x} = \frac{1}{n} \sum_{j=1}^{n} x_j^{mean} \quad \text{Eq. 5}$$

where $\hat{x}$ is the result of the measurement and n the number of repeated tests j.

Then the type A standard uncertainty U_A is calculated as follows:

$$U_A = \sqrt{\frac{1}{n-1} \sum_{j=1}^{n} (x_j^{mean} - \hat{x})^2} \quad \text{Eq. 6}$$

(iii) Finally, the combined standard uncertainty U_C of the measurement is calculated as follows (JCGM, 2008; Taylor and Kuyatt, 1994):

$$U_C = \sqrt{{U_A}^2 + {U_B}^2} \quad \text{Eq. 7}$$

A new campaign of 10 repeated tests was carried out under the same conditions on speckled coupons to analyse the possible improvement of this artificial speckling as compared with the natural pattern intrinsic to the leaflet tissues of both species. To do so, the Python package SciPy (Virtanen et al., 2020) was used to carry out Wilcoxon test between paired coupons, either with or without speckle.

2.4. Comparison of DIC with laser extensometry

A comparison with laser extensometry was conducted to assess the accuracy of DIC. This validation, also called triangulation, was performed by using the same measurand on the same set of coupons (JCGM, 2012; Nelson et al., 2019). Tensile tests based on laser extensometry were carried out at IMT Mines Ales, using a tensile bench (MTS Criterion C45.105) equipped with pneumatic jaws and a 1 kN sensor, coupled to a laser extensometer (MTS laser extensometer LX500) (Fig. 2b). Displacement speed, force acquisition rate, preload and maximum loading were exactly the same as for the DIC experiments. Coupons were equipped with reflective tape markers to track uniaxial deformation during the test. The gauge length, i.e. the initial distance between the markers, was set at 50 mm, corresponding to the ROI used for DIC. The overall axial strain ε_{yy} was obtained from the relative change in marker distance. Elastic modulus (E_y) was calculated following Eq.1 over the same strain range as DIC (from 0.05% to 0.2%). To compare DIC with laser extensometry, the average axial strain ε_{yy} (along the loading

direction) of the 60 coupons was calculated over the ROI as the mean of the longitudinal strains of all subsets through DIC, and compared with the unique overall strain value measured by the laser extensometry technique on the same coupon. Mild outliers of ε_{yy} measurements (measured by either DIC or laser extensometry) were discarded using interquartile range (IQR)-based methods with Tukey fences set at 1.5 x IQR (Dastjerdy et al., 2023). After filtering, 58 coupons were retained (29 *Euterpe oleracea* and 29 *Oenocarpus bataua*). In order to compare ε_{yy} measurements from both measurement methods under equivalent stress conditions, three common levels of stress were defined. The common minimum and maximum of stress registered for DIC (σ_{DIC}) and for laser extensometry (σ_{ext}) were determined as:

$$\sigma_{\min} = \max(\min(\sigma_{ext}), \min(\sigma_{DIC})) \quad \text{Eq. 8}$$

$$\sigma_{\max} = \min(\max(\sigma_{ext}), \max(\sigma_{DIC})) \quad \text{Eq. 9}$$

Then, three levels of stress σ_k were calculated using a factor α corresponding to low, mid and high stress values:

$$\alpha = \{0.1, \quad 0.5, \quad 0.9\}$$

$$\sigma_k = \quad \sigma_{\min} + \alpha_k(\sigma_{\max} - \sigma_{\min}) \quad \text{Eq. 10}$$

For each stress level σ_k, the corresponding ε_{yy} was determined by using the closest experimental points i_k for laser extensometry and j_k for DIC:

$$i_k = \underset{i}{\arg\min}|\sigma_{ext}(i) - \sigma_k|, \quad j_k = \underset{j}{\arg\min}|\sigma_{DIC}(j) - \sigma_k| \quad \text{Eq. 11}$$

$$\varepsilon_{ext}^{(k)} = \varepsilon_{ext}(i_k), \quad \varepsilon_{DIC}^{(k)} = \varepsilon_{DIC}(j_k)$$

Because both measurement tests were subject to errors, the correlation of ε_{yy} measurements for DIC and laser extensometry was evaluated using a type II regression using RMA (Reduced Major Axis) with the SciPy package. The RMA slope reflects the variability of both methods, rather than the OLS (Ordinary Least Squares) regression (Smith, 2009). To evaluate the relation between both methods, the Pearson's correlation coefficient (r) was reported. The modulus of elasticity *Ey*, was calculated for each coupon with ε_{yy} measurements from DIC and laser extensometry, as detailed in Eq.1. Then, a statistical analysis for paired data was performed using the Wilcoxon rank test from the SciPy.stats package (Virtanen et al., 2020) to determine whether relative differences between the two tests are significant for ε_{yy} and *Ey*.

2.5. Inter-specific variability via DIC

To assess interspecific differences in E_y and ν_{yx}, 58 coupons were used (29 *Euterpe oleracea* and 29 *Oenocarpus bataua*) using DIC. Coupons with negative Poisson's ratios were discarded from the calculation of ν_{yx}, resulting in 46 coupons (27 *Euterpe oleracea* and 19 *Oenocarpus bataua*). For each species, the mean, the standard deviation (SD), and the coefficient of variation (CV) were reported. The CV indicates the relative variability within each species and was calculated as the SD divided by the absolute value of the mean.

Interspecific differences in E_y and ν_{yx} were evaluated using a Mann-Whitney *U* test, implemented with the Python package SciPy.stats (Virtanen et al., 2020).

2.6. Heterogeneity in full-field deformation and edge effects

Heterogeneity in the full-field deformation and potential edge effects were visualised using heatmaps and quantified by estimating local ε_{xx}, ε_{yy}, and Poisson's ratio in nine equal subareas of the ROI. To assess differences between edges and central zones a Wilcoxon signed-rank test was applied using the Python package SciPy.stats (Virtanen et al., 2020). Poisson's ratio was computed via ordinary least squares regression as described in Eq. 2, and the coefficient of determination (R^2) was used to evaluate the quality of the fit. Interspecific differences among central areas were assessed using the Mann-Whitney test.

2.7. Histological analysis and its relationship with DIC-derived biomechanical properties

A subset of 26 coupons (10 *Euterpe oleracea* – 16 *Oenocarpus bataua*) was used to carry out histological analysis. Image acquisition of thin leaflet sections stained with FASGA was carried out at the AMAP (botany and Modeling of Plant Architecture and vegetation) technical platform. The staining enabled discrimination of cellulosic tissues (blue) to lignified tissues (red magenta), thereby highlighting vascular bundles (Fig. 4a). Embedding, sectioning, staining and numerical imaging procedure followed the recently published protocol by Fonti et al. (2025). For separating and quantifying the vascular bundles which have been reported to influence tensile strength and stiffness of plant tissues (Fathi and Frühwald, 2014; Gibson, 2012; Li et al., 2024; Li and Shen, 2011; Zhai et al., 2013), image analysis was performed using ImageJ software (Schneider et al., 2012). Then, the extraction process allowed discrimination of leaflet area, vascular bundle area and lumen area (within the bundles), all measured in pixels (Fig. 4). The bundle fraction was defined as the ratio of the bundle area to the leaflet area. The wall fraction was calculated as the ratio of the bundle wall area (difference between bundle and lumen areas) to the leaflet area. Finally, the bundle wall fraction was defined as the ratio of the wall area with the bundle area.

To assess the relationship between DIC-derived strain field and leaflet microstructure, the relationships between anatomical features and mechanical properties were analysed using OLS regression.

3. Results & discussion

3.1. Systematic error and standard uncertainty

The systematic error (ϵ_s) of the camera resulted in a discrete deformation field matrix of size [136 × 19 + /- 1 nodes]. The systematic error (ϵ_s) was in the range [5×10^{-08} - 1.48×10^{-05}] for ε_{yy} and [5×10^{-06} - 1.09×10^{-04}] for ε_{xx}. Despite the natural variability of palm tree leaflets, these values were comparable to previous studies on an aluminium coupon reported in the range [5×10^{-06} – 1×10^{-03}] (Haddadi and Belhabib, 2008; Iliopoulos and Andrianopoulos, 2010). These results confirmed that the DIC strain measurement method exhibited low values of systematic error. Furthermore, the systematic error of ε_{yy} and ε_{xx} was equal to or lower than type B standard uncertainty (U_B), indicating that no correction was needed to compensate (summarised results are provided in Supplementary Table A.1). The combined standard uncertainty (U_C) ranged from [3.9×10^{-5} - 2.57×10^{-4}] for ε_{yy} and [6×10^{-5} - 3.32×10^{-3}] for ε_{xx}. These values were similar to those reported in previous studies on aluminium coupons with a standard uncertainty value of [2.11×10^{-5} – 5×10^{-4}] for ε_{yy} (Badaloni et al., 2015; Das et al., 2021; Iliopoulos and Andrianopoulos, 2010). These comparisons with our results underlined the accuracy and repeatability of the method.

Although the positive effect of the speckle pattern on the accuracy of the displacement recordings is well established (Dong and Pan, 2017; Lecompte et al., 2006; LePage et al., 2017; Szalai et al., 2023), no significant difference was observed between speckled and non-speckled coupons either for ε_{yy} (p-value = 0.18) nor ε_{xx} (p-value = 1) (See distribution of the standard deviation, Supplementary Fig.A3). Similarly, E_y did not differ significantly between coupons with and without speckling (respectively 2628 MPa and 2601 MPa, paired *t*-test, *t*-stat = −0.81, p-value = 0.44). As demonstrated by Sánchez-Arévalo and Pulos (2008), some materials naturally exhibit random speckle patterns, as was the case with the palm leaflets tested, making speckling unnecessary.

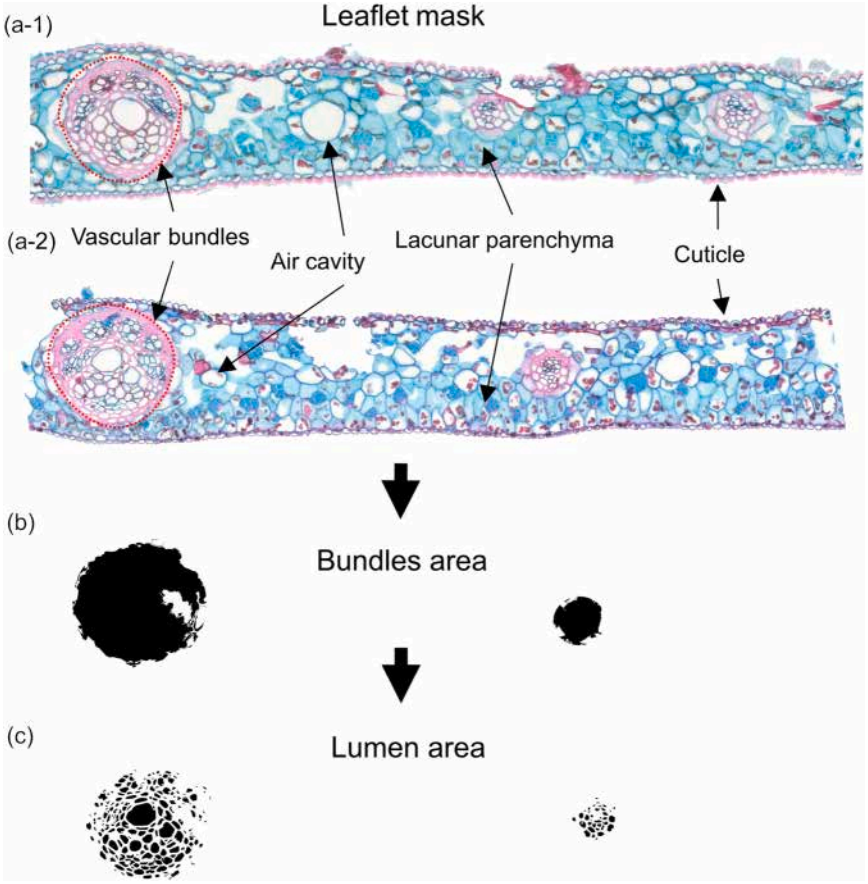

Fig. 4. Segmentation process of the FASGA stained leaflet section numerical images: (a) thin section of two palm species stained with FASGA, highlighting cellulosic tissues in blue and lignified tissues in red magenta; (a-1) *Euterpe oleracea;* (a-2) *Oenocarpus bataua;* (b) extraction of the vascular bundles from the leaflet mask of Oenocarpus bataua with the software ImageJ; (c) extraction of the lumen from the vascular bundles of Oenocarpus bataua.

3.2. DIC vs laser extensometry

Paired Wilcoxon rank test revealed significant difference between the two measurements methods (p-value $< 10^{-8}$), indicating a systematic bias between DIC and laser extensometer. For the same level of stress, ε_{yy} from DIC tended to be higher than those from laser extensometry with an estimated slope RMA of 1.16 and an intercept of 4.99×10^{-3} with p-value $< 10^{-26}$ (Fig. 5). The lower slope (0.82) and higher intercept (5.53×10^{-2}) with p-value $< 10^{-26}$ calculated from OLS regression (Fig. 5) showed that variability arises from errors affecting both measurement techniques rather than from a systematic bias of DIC. Nevertheless, a significant correlation was observed ($r = 0.71$, p-value $< 10^{-26}$) highlighting consistent covariation of ε_{yy} measurements across stress levels.

A comparison of *Ey* values from DIC and laser extensometer was done for the two species, *Euterpe oleracea* and *Oenocarpus bataua*. For both species, the mean *Ey* values were slightly lower with the DIC method compared to the laser extensometer, however no significant differences were found between the two methods (Table 1). These differences appeared to be small relative to the variability reported in other studies on plant fibres. In a benchmark study on the mechanical properties of single fibres, Jeannin et al. (2024) showed that the elastic modulus measured in different laboratories on the same type of fibre could give significant variability of values. The primary sources of variation were operator-dependent factors (fibre selection and handling), and experimental protocols (e.g., cross-sectional measurement). The authors also emphasized that image correlation can reduce uncertainties in strain measurements caused by frame compliance and/or slippage in grips.

In line with the first hypothesis, DIC demonstrated high accuracy by providing strain measurements consistent with laser extensometer. This validates its robustness for complex, fibrous biological materials where local heterogeneity challenges conventional approaches.

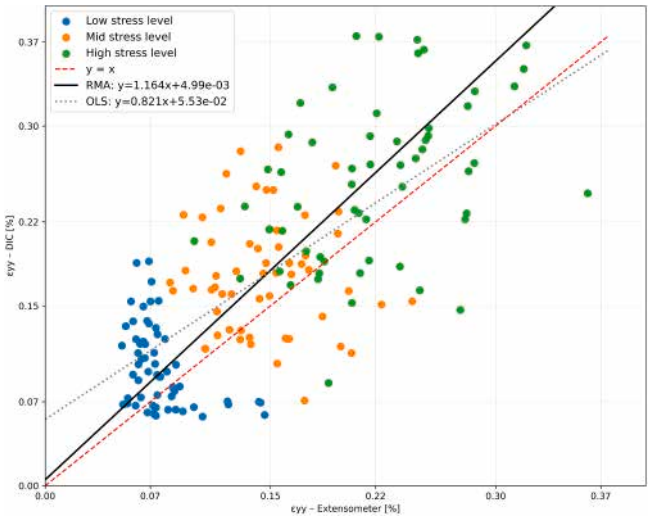

Fig. 5. Comparison of two strain measurement methods through type II linear regression (Reduced Major Axis). The plot shows ε_{yy} measured by DIC versus ε_{yy} measured by laser extensometer with type II linear regression, ordinary least-squares regression and the identity line $y = x$. Levels of stress were defined for each strain measurement and are coloured in the plots.

Table 1
Comparison of Ey measured by DIC and laser extensometer for two palm species: *Oenocarpus bataua* and *Euterpe oleracea*. Values are expressed as mean ± standard deviation (SD). The number of coupons is indicated and the p-value corresponds to the statistical comparison between the two methods.

Species (58)	*Ey* mean [MPa] DIC	*Ey* mean [MPa] Laser extensometer	p-value
Oenocarpus bataua (29)[a]	1730 ± 463[b] (26)[c]	1834 ± 516 (28)	0.16
Euterpe oleracea (29)	2194 ± 486 (22)	2369 ± 698 (29)	0.15

[a] Number of coupons is indicated in brackets
[b] Standard deviation [MPa]
[c] Coefficient of variation [%] is indicated in brackets

3.3. Potential of DIC for assessing inter-specific variability

DIC confirmed its ability to unveil differences in mechanical properties between two morphologically distinct species. The stress–strain curves measured via DIC within the elastic domain of the 58 coupons are shown in Fig. 6. The DIC method exhibited relatively lower coefficient of variation than laser extensometry suggesting that it provides more precise measurements (Table 1). *Ey* showed significant interspecific differences (Mann-Whitney U-test, $z = 5.88$, $p < 10^{-8}$), with a mean of 2194 MPa for *Euterpe oleracea* (29 coupons) and 1730 MPa for *Oenocarpus bataua* (29 coupons). Such a high level of dispersion is characteristic of biological cellular materials (Alméras et al., 2024; Gibson, 2012; Green et al., 2010; Li et al., 2024; Miyoshi et al., 2018; Niklas and Spatz, 2010). Plant tissues behave as anisotropic fibre-reinforced composites whose mechanical properties strongly depend on anatomical organization and the microfibrillar angle distribution in cell walls, leading to naturally high coefficients of variation. The observed variability therefore represents intrinsic biological heterogeneity rather than experimental uncertainty. These results also suggest that DIC is sufficiently accurate to detect inter-specific variations in heterogeneous plant materials.

Although elastic modulus values in the literature are generally derived from individual fibres extracted from leaflet, the values reported here (~2 GPa) are consistent with those of other palm fibres such as coir (3 – 17 GPa) (Bourmaud et al., 2018; Tomczak et al., 2007) and piassava fibres (1 – 7 GPa) (d'Almeida et al., 2006; Müssig, 2010). These values are comparable to other lignocellulosic materials such as cotton (5.5 – 13 GPa), silk (3 – 10 GPa) and wool (2.3 – 5 GPa) (Pickering et al., 2016).

Stress–strain curves showed a shift in ε_{xx} for some coupons, leading to negative Poisson's ratio, which is unexpected for such biological materials (See Supplementary Fig.A4). These aberrant values likely arise from out-of-plane motion and edge effect due to the curvature of the coupons. These negative values were thus excluded, resulting in a dataset of 46 coupons (27 *Euterpe oleracea* and 19 *Oenocarpus bataua*). Poisson's ratio of the two species differed significantly (Mann-Whitney *U*-test, $z = -4.14$, p-value $< 10^{-4}$) with a mean of 0.27 for *Euterpe oleracea* and 0.98 for *Oenocarpus bataua*, indicating contrasted behaviours between the two species.

Oenocarpus bataua showed a wide dispersion of Poisson's ratio values, sometimes exceeding 0.5, which is not common compared with values reported in previous studies (Greaves et al., 2011; Hua et al., 2020; Lu et al., 2022). As shown in Fig. 6, *Oenocarpus bataua* showed high ε_{xx} values relative to σ_{yy}. Although recent studies reported high Poisson's ratio for natural fibre materials (Alméras et al., 2024) such values may also arise from artefacts during image acquisition (edge effects and out-of-plane motions, see 3.4).

In general, the quality of the regression was satisfactory, with R^2 values exceeding 0.7 for all coupons except seven *Euterpe oleracea* and one *Oenocarpus bataua*.

3.4. Heterogeneity in full-field deformation and edge effects

DIC offers the opportunity to generate full-field deformation heatmaps, which enable visualization of spatial heterogeneity and to identify edge effects (Fig. 7).

Strain values along the y-axis were slightly higher at the top and bottom of the coupon, close to the grips, while absolute strain values along the x-axis were considerably higher at the edge of the coupon, indicating a potential edge effect. Spatial heterogeneity was quantified for each of the nine subareas *a* to *i* (Fig. 8).

While the mean ε_{yy} was relatively uniform across subareas, the mean ε_{xx} was higher at the edge of the ROI (subareas {a, c, d, f, g, i}) than in the centre of the coupon (subareas {b, e, h}), suggesting potential edge effects (see Supplementary Fig.A5). A statistical comparison using the Wilcoxon test showed significant differences between edges and central subareas for ε_{xx} (p-value $< 10^{-5}$), while ε_{yy} showed minor differences (p-value = 0.05). Central subareas {b, e, h} were then used to evaluate how Poisson's ratios vary locally in non-edge subareas. Within the central subareas, only ε_{yy} values in range [0.002–0.008] were considered to reduce the occurrence of negative Poisson's ratios. However, rather than computing Poisson's ratios -which assume elastic behaviour- comparisons were based on ε_{xx} and ε_{yy} values directly. Within this interval only seven negative values for subareas *b* and *h* (n = 58) and eight for subarea *e* (n = 57) were observed. Analysis of the OLS regressions revealed that

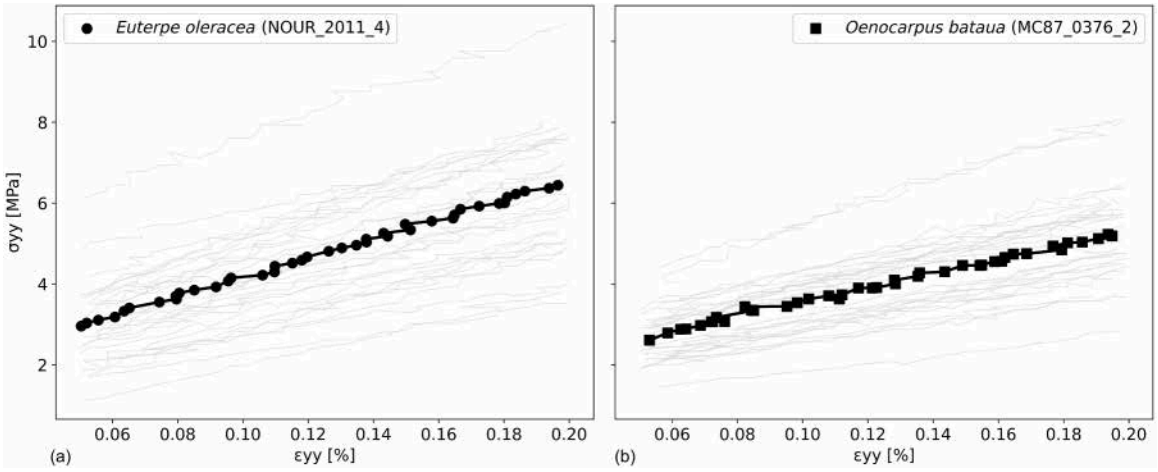

Fig. 6. Illustration of the σ_{yy} - ε_{yy} curves measured via DIC within the elastic domain for a subset of 58 coupons. One representative coupon is highlited by dots for two species of palms: (a) *Euterpe oleracea* (circle dots) (b) *Oenocarpus bataua* (square dots).

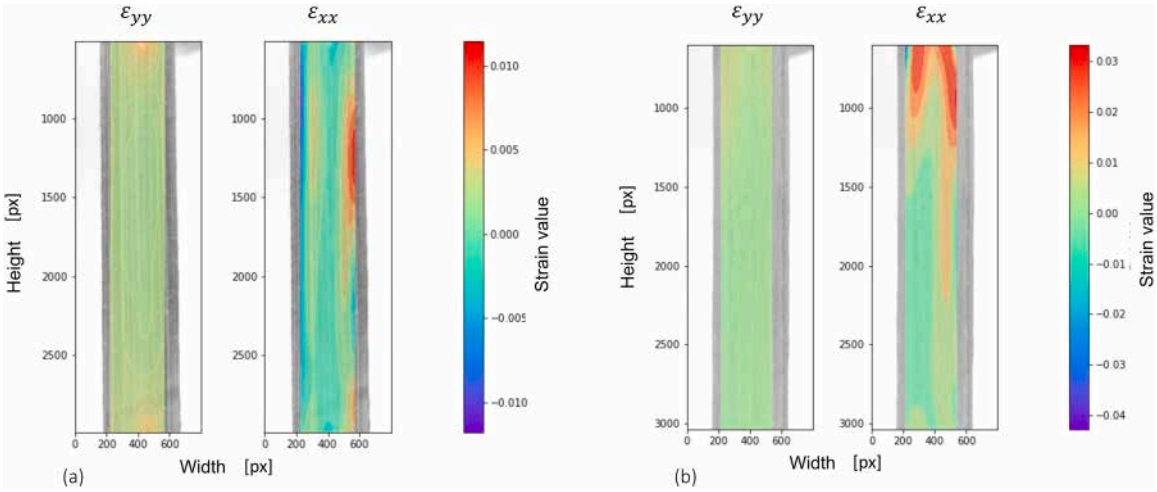

Fig. 7. Illustration of the edge effect through full-field deformation heatmaps of ε_{yy} (leftside) and ε_{xx} (rightside), of two representative coupons: (a) *Euterpe oleracea* (b) *Oenocarpus bataua*.

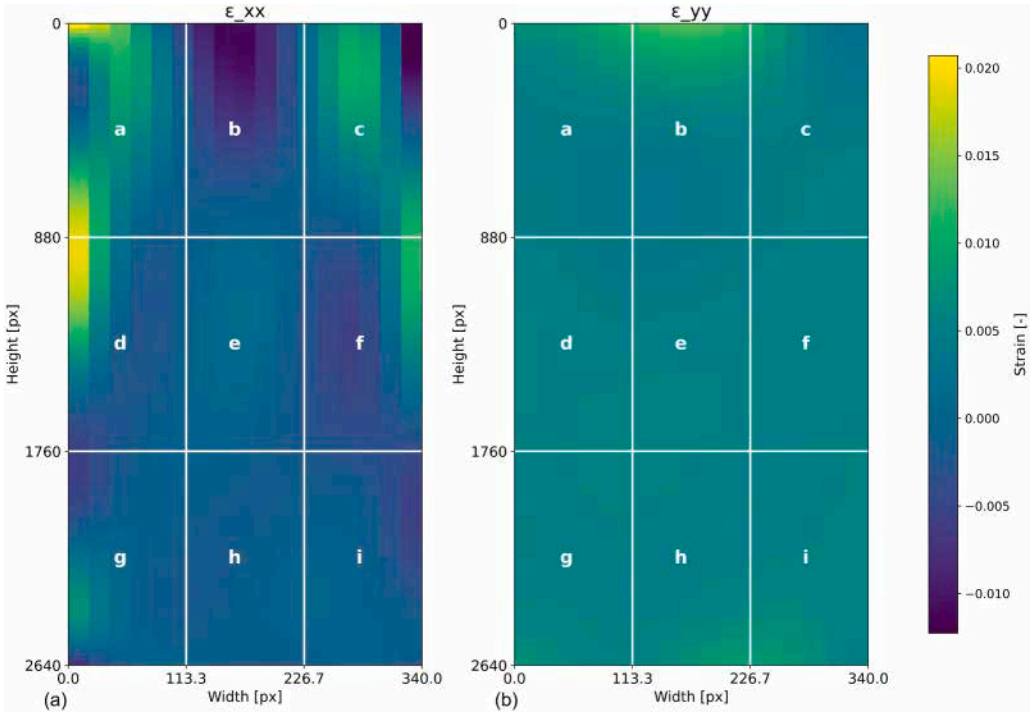

Fig. 8. Representative heatmap of full-field deformation of a Euterpe oleracea leaflet coupon divided into nine subareas (labelled a-i). (a) Heatmap of full-field deformation of εxx (b) Heatmap of full-field deformation of εyy.

subareas *b* and *e* had nine coupons (7 *Euterpe oleracea,* 2 *Oenocarpus bataua*) with R^2 values below 0.6, while subarea *h* had seven coupons (5 *Euterpe oleracea,* 2 *Oenocarpus bataua*). While *Euterpe oleracea* exhibited similar dispersion across the three central subareas, *Oenocarpus bataua* showed heterogeneous results, with higher variability concentrated in subarea *e* (Fig. 9). As a result, only subarea *e* displayed a significant difference between species (Mann-Whitney test, p-value $< 10^{-3}$). Taken together, these results showed that edge-related artefacts, such as coupons curvature and out-of-plane motion, were mitigated by restricting the analysis to the central subareas of the ROI. However, intrinsic heterogeneity in the material remained in the central zones. Furthermore, a significant difference between the two species was observed in subarea *e* (Fig. 9).

These results supported the advantages of DIC for evidencing the spatial heterogeneity of deformation in plant tissues.

3.5. Relationship between anatomical features and modulus of elasticity

Although the relationship between vascular bundle density and *Ey* is well known for woody structure (Gibson and Ashby, 1988; Miyoshi et al., 2018; Niklas and Spatz, 2010), it remains poorly documented in palm leaves. First, the analysis of the relationship between density and *Ey* of leaflets over the 58 coupons showed no significant global correlation, whereas significant positive correlation was found when analysing the two species separately (Table 2). This suggests that density cannot explain differences in *Ey* between species, although it remained a good predictor within each species.

The analysis of the relationships between anatomical features and *Ey*

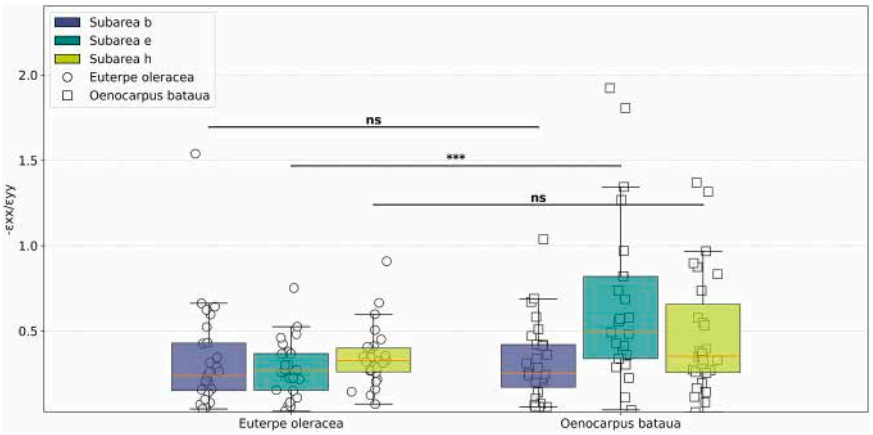

Fig. 9. Strain ratio of Euterpe oleracea and Oenocarpus bataua of three centred subareas {b, e, h}. A significant difference between species was detected in subarea e using the Mann-Whitney test ($p < 10^{-3}$).

Table 2
Global analysis of Ey versus anatomical features for two palm species: Oenocarpus bataua and Euterpe oleracea. The number of coupons is indicated. The coefficient of correlation and determination from the ordinary least squares regression and the corresponding p-value are reported.

Analysis	Species (n)	r	p-value
Ey vs Density	Global (58)	0.08	0.55
	Euterpe oleracea (29)	0.43	1.91×10^{-2}
	Oenocarpus bataua (29)	0.51	4.53×10^{-3}
Ey vs Bundles fraction	Global (26)	0.44	2.39×10^{-2}
	Euterpe oleracea (10)	0.44	0.2
	Oenocarpus bataua (16)	0.41	0.11
Ey vs wall fraction	Global (26)	0.27	0.18
	Euterpe oleracea (10)	0.19	0.6
	Oenocarpus bataua (16)	0.34	0.2
Ey vs bundles wall fraction	Global (26)	- 0.3	0.14
	Euterpe oleracea (10)	- 0.79	7×10^{-3}
	Oenocarpus bataua (16)	0.09	0.74

was performed on a subset of 26 coupons. Only the relationship between *Ey* and the bundles fraction showed a global positive correlation ($r = 0.44$, p-value $= 2.39 \times 10^{-2}$). The relationship between *Ey* and the wall fraction showed no significant correlation. A strong negative significant correlation between *Ey* and the bundles wall fraction was observed only for *Euterpe oleracea* ($r = -0.79$, p-value $= 7 \times 10^{-3}$). These preliminary results, thus highlight interspecific structural differences between the two species but require further investigation to elucidate anatomical/structural and mechanical relationships in palm leaflets. It should also be noticed that *Euterpe oleracea* coupons were difficult to stain, which often resulted in tissue damage.

3.6. Experimental biases and limits of DIC

Although DIC has proven effective in characterizing the mechanical behaviour of palm leaflets, several steps are crucial to minimize measurement errors and discard outliers. This procedure can be divided into two stages, pre- and post-testing, respectively. During the pre-test stage, the experimenter must carefully prepare the coupon and position it within the grips before applying a preload. Improper coupon positioning can cause leaflet curvature, leading to portions of the coupon falling outside the camera's field of view. When tension is applied, the coupon may unfold, introducing an offset in the strain ε_{xx}. Such an out-of-plane effect can produce aberrant Poisson's ratios (negative values). In addition, defining an appropriate strain range is important to exclude the initial non-linear part of the curve. These observations also emphasize the importance of carefully selecting the region of interest (ROI) and assessing such biases *a posteriori*.

During the post-test stage, the analyser should apply suitable filtering depending on which properties are evaluated. At a minimum, we recommend filtering aberrant values with the IQR method, or other equivalent approaches. It is also important to verify results with a graphical analysis in order to support the decision to filter or reduce ROI of a given coupon.

Here, we recommend using the local Poisson's ratio versus the longitudinal strain coupled with the heatmap distribution of ε_{xx} and ε_{yy} values to make such decision. In addition, this analysis should be complemented by dividing the ROI to identify and remove edge-related artefacts.

Once these artefacts are excluded, the remaining data can be interpreted as true spatial variation of the coupon. In this context, DIC's spatial resolution enables localized mechanical characterization, which is often missed by global measurements. This is particularly relevant for anisotropic or structurally heterogeneous biological materials, where local mechanical properties can vary significantly within the same coupon. Further improvements, such as deep learning DIC (Yang et al., 2022) or the use of 3D-DIC (Fischer et al., 2024; Mylo and Poppinga, 2023), could help better understand these phenomena and further minimize these artefacts, providing an even more accurate assessment of spatial heterogeneity in the mechanical response.

4. Conclusion

This study highlights that DIC is a powerful and accurate method that can be reliably applied to heterogeneous plant materials, such as palm leaflets. Indeed, DIC demonstrated its robustness and repeatability for assessing strain and elasticity, with minimal systematic error and standard uncertainties. The deformation values measured with DIC closely aligned with those measured using a conventional laser extensometer, and the range of elasticity values was consistent with those reported for other plant materials in the literature. Importantly, DIC offers advantages over laser extensometry by enabling full-field strain analysis, allowing for the observation of spatial heterogeneity in mechanical behaviour, and the extraction of additional parameters – such as Poisson's ratio – that are inaccessible through conventional uniaxial measurements. Additionally, the growing interest in DIC, along with recent advances such as stereo image correlation, can help to overcome edge effects and enhance measurement accuracy further, thereby broadening its applicability to complex plant materials.

Beyond methodological validation, this study finally provides the first quantitative estimates of mechanical properties for Amazonian palm leaflets, contributing novel biomechanical data for two culturally and economically important but under-documented species. This study thus opens new perspectives for both fundamental plant biomechanics

and the valorisation of sustainable bio-based materials.

Author contributions

LB, JE & PC: Collected the palm samples. PC, SC, RLEG, RLEH, NLM: Carried-out the experiments. PC, RLEH & DA: Wrote the codes. RLEH, JB & LB: Supervised the work. All authors wrote the manuscript

CRediT authorship contribution statement

Paul Cathelineau: Writing – review & editing, Writing – original draft, Visualization, Validation, Software, Resources, Methodology, Formal analysis, Data curation. **Julie Bossu:** Writing – review & editing, Validation, Supervision. **Julien Engel:** Writing – review & editing, Resources. **Romain Lehnebach:** Writing – review & editing, Supervision, Software, Investigation. **Louise Brousseau:** Writing – review & editing, Resources, Project administration, Funding acquisition, Conceptualization, Supervision. **Damien André:** Writing – review & editing, Software. **Stéphane Corn:** Writing – review & editing, Investigation. **Romain Léger:** Writing – review & editing, Investigation. **Nicolas Le Moigne:** Writing – review & editing, Investigation.

Funding

DOPAMICS is funded by the European Union (ERC, grant no. 101039272). Views and opinions expressed are those of the author(s) only and do not necessarily reflect those of the European Union or the European Research Council Executive Agency (ERCEA). Neither the European Union nor the granting authority can be held responsible for them.

Declaration of Competing Interest

The authors declare that they have no known competing financial interests or personal relationships that could have appeared to influence the work reported in this paper.

Acknowledgements

The authors are grateful to the institutions that supported and facilitated this study. We acknowledge the Nouragues Ecological Research Station (CNRS), which benefits from 'Investissement d'Avenir' grants managed by the Agence Nationale de la Recherche (AnaEE France ANR-11-INBS-0001; Labex CEBA ANR-10-LABX-25–01), and the National Forests Office (ONF) in French Guiana for granting access to the study sites. This work also received support from the French National Research Agency (CEBA, ref. ANR-10-LABX-25–01). We also thank the C2MA laboratory of the Institut Mines-Alès for providing access to research infrastructures and equipment.

Appendix A. Supporting information

Supplementary data associated with this article can be found in the online version at doi:10.1016/j.indcrop.2026.123248.

Data availability

Data will be made available on request.

References

Alméras, T., Corn, S., Baranger, A., Regazzi, A., Barés, J., Lehnebach, R., Clair, B., 2024. Extreme Poisson's ratios recorded in the secondary phloem of Malvaceae: a highlight on the biomechanical function of bark. Trees Struct. Funct. 1379–1390. https://doi.org/10.1007/s00468-024-02558.

Al-Zube, L.A., Robertson, D.J., Edwards, J.N., Sun, W., Cook, D.D., 2017. Measuring the compressive modulus of elasticity of pith-filled plant stems. Plant Methods 13 (1). https://doi.org/10.1186/s13007-017-0250-y.

Al-Zube, L., Sun, W., Robertson, D., Cook, D., 2018. The elastic modulus for maize stems. Plant Methods 14 (1). https://doi.org/10.1186/s13007-018-0279-6.

André, D. (2017). Pydic. ⟨https://gitlab.com/damien.andre/pydic⟩.

Atkinson, G., & Nevill, A.M. (1998). Statistical Methods For Assessing Measurement Error (Reliability) in Variables Relevant to Sports Medicine. Sports Med. https://doi.org/10.2165/00007256-199826040-00002.

Badaloni, M., Rossi, M., Chiappini, G., Lava, P., Debruyne, D., 2015. Impact of experimental uncertainties on the identification of mechanical material properties using DIC. Exp. Mech. 55 (8), 1411–1426. https://doi.org/10.1007/s11340-015-0039-8.

Bao, T., Melenka, G.W., Ljubotina, M.K., Carey, J.P., Cahill, J.F., 2018. A new method for the rapid characterization of root growth and distribution using digital image correlation. N. Phytol. 218 (2), 835–846. https://doi.org/10.1111/nph.15009.

Bernal, R., Torres, C., García, N., Isaza, C., Navarro, J., Vallejo, M.I., Galeano, G., Balslev, H., 2011. Palm management in South America. Bot. Rev. 77 (Number 4), 607–646. https://doi.org/10.1007/s12229-011-9088-6.

Bidhendi, A.J., Geitmann, A., 2018. Tensile testing of primary plant cells and tissues. Springer Verlag. https://doi.org/10.1007/978-3-319-79099-2_15.

Blaysat, B., Grédiac, M., Sur, F., 2016. On the propagation of camera sensor noise to displacement maps obtained by DIC - an experimental study. Exp. Mech. 56 (6), 919–944. https://doi.org/10.1007/s11340-016-0130-9.

Bourmaud, A., Beaugrand, J., Shah, D.U., Placet, V., Baley, C., 2018. Towards the design of high-performance plant fibre composites. Prog. Mater. Sci. 97, 347–408. https://doi.org/10.1016/j.pmatsci.2018.05.005.

Cámara-Leret, R., Faurby, S., Macía, M.J., Balslev, H., Göldel, B., Svenning, J.C., Kissling, W.D., Rønsted, N., Saslis-Lagoudakis, C.H., 2017. Fundamental species traits explain provisioning services of tropical American palms. Nat. Plants 3. https://doi.org/10.1038/nplants.2016.220.

Cámara-Leret, R., Paniagua-Zambrana, N., Balslev, H., Macía, M.J., 2014. Ethnobotanical knowledge is vastly under-documented in northwestern South America. PLoS ONE 9 (1). https://doi.org/10.1371/journal.pone.0085794.

Cheng, S., Clarke, E.C., Bilston, L.E., 2009. The effects of preconditioning strain on measured tissue properties. J. Biomech. 42 (9), 1360–1362. https://doi.org/10.1016/j.jbiomech.2009.03.023.

Cheng, P., Sutton, M.A., Schreier, H.W., Mcneill, S.R., 2002. Full-field speckle pattern image correlation with B-spline deformation function. Exp. Mech. 42, 344–352. https://doi.org/10.1007/BF02410992.

Coelho, S.D., Levis, C., Baccaro, F.B., Figueiredo, F.O.G., Antunes, A.P., ter Steege, H., Peña-Claros, M., Clement, C.R., Schietti, J., 2021. Eighty-four per cent of all Amazonian arboreal plant individuals are useful to humans, 10 October PLoS ONE 16. https://doi.org/10.1371/journal.pone.0257875.

Couvreur, T., Baker, W., 2013. Tropical rain forest evolution: palms as a model group. BMC Biol. 11, 48. https://doi.org/10.1186/1741-7007-11-48.

d'Almeida, J.R.M., Aquino, R.C.M.P., Monteiro, S.N., 2006. Tensile mechanical properties, morphological aspects and chemical characterization of piassava (Attalea funifera) fibers. Compos Part A Appl Sci Manuf 37, 1473–1479. https://doi.org/10.1016/j.compositesa.2005.03.035.

Dahle, G.A., 2017. Influence of bark on the mapping of mechanical strain using digital image correlation. Wood Sci. Technol. 51 (6), 1469–1477. https://doi.org/10.1007/s00226-017-0947-0.

Das, P.P., Elenchezhian, M.R.P., Vadlamudi, V., Reifsnider, K., Raihan, R., 2021. RealPi2dDIC: A Low-cost and open-source approach to in situ 2D digital image correlation (DIC) applications. SoftwareX 13. https://doi.org/10.1016/j.softx.2020.100645.

Dastjerdy, B., Saeidi, A., Heidarzadeh, S., 2023. Review of Applicable Outlier Detection Methods to Treat Geomechanical Data. In: Geotechnics, 3. Multidisciplinary Digital Publishing Institute (MDPI), pp. 375–396. https://doi.org/10.3390/geotechnics3020022.

Dierckx, P., 1981. An Algorithm for Surface-Fitting with Spline Functions. IMA J. Numer. Anal. 1. https://doi.org/10.1093/imanum/1.3.267.

Dong, Y.L., Pan, B., 2017. A Review of Speckle Pattern Fabrication and Assessment for Digital Image Correlation. Exp. Mech. 57 (8), 1161–1181. https://doi.org/10.1007/s11340-017-0283-1.

Eiserhardt, W.L., Svenning, J.C., Kissling, W.D., Balslev, H., 2011. Geographical ecology of the palms (Arecaceae): Determinants of diversity and distributions across spatial scales. Ann. Bot. 108 (Number 8), 1391–1416. https://doi.org/10.1093/aob/mcr146.

Fathi, L., Frühwald, A., 2014. The role of vascular bundles on the mechanical properties of coconut palm wood. Wood Mater. Sci. Eng. 9 (4), 214–223. https://doi.org/10.1080/17480272.2014.887774.

Fayad, S.S., Seidl, D.T., Reu, P.L., 2020. Spatial DIC Errors due to Pattern-Induced Bias and Grey Level Discretization. Exp. Mech. 60 (2), 249–263. https://doi.org/10.1007/s11340-019-00553-9.

Fischer, M., Mylo, M.D., Lorenz, L.S., Böckenholt, L., Beismann, H., 2024. Stereo Camera Setup for 360° Digital Image Correlation to Reveal Smart Structures of Hakea Fruits. Biomimetics 9 (3). https://doi.org/10.3390/biomimetics9030191.

Fonti, M.V., Von Arx, G., Harroue, M., Schneider, L., Nievergelt, D., Björklund, J., Hantemirov, R., Kukarskih, V., Rathgeber, C.B.K., Studer, N.-T., Fonti, P., 2025. A Protoc. High. -Qual. Sect. tree-ring Anat. https://doi.org/10.3389/fpls.2025.1505389ï.

Gibson, L.J., 2012. The hierarchical structure and mechanics of plant materials. In: Journal of the Royal Society Interface, 9. Royal Society, pp. 2749–2766. https://doi.org/10.1098/rsif.2012.0341.

Gibson, L.J., Ashby, 1988. Cellular solids - structure and properties. Gibson and Ashby, 1988. Cambridge University Press.
Granville, J.J. De. (1999). Palms of French Guiana: diversity, distribution, ecology and uses. ⟨https://www.jstor.org/stable/44652967⟩.
Greaves, G.N., Greer, A.L., Lakes, R.S., Rouxel, T., 2011. Poisson's ratio and modern materials. In: Nature Materials, 10. Nature Publishing Group, pp. 823–837. https://doi.org/10.1038/nmat3134.
Green, D.W., Winandy, J.E., Kretschmann, D.E., 2010. Mechanical Properties of Wood. Forest Products Laboratory. Wood handbook. Chapter 4.
Haddadi, H., Belhabib, S., 2008. Use of rigid-body motion for the investigation and estimation of the measurement errors related to digital image correlation technique. In: Optics and Lasers in Engineering, 46, pp. 185–196. https://doi.org/10.1016/j.optlaseng.2007.05.008.
Harris, C.R., Millman, K.J., van der Walt, S.J., Gommers, R., Virtanen, P., Cournapeau, D., Wieser, E., Taylor, J., Berg, S., Smith, N.J., Kern, R., Picus, M., Hoyer, S., van Kerkwijk, M.H., Brett, M., Haldane, A., del Río, J.F., Wiebe, M., Peterson, P., Oliphant, T.E., 2020. Array programming with NumPy. In: Nature, 585. Nature Research, pp. 357–362. https://doi.org/10.1038/s41586-020-2649-2.
Heijink, B.M., McMichael, C.N.H., Piperno, D.R., Duivenvoorden, J.F., Cárdenas, D., Duque, Á., 2020. Holocene increases in palm abundances in north-western Amazonia. J. Biogeogr. 47 (3), 698–711. https://doi.org/10.1111/jbi.13721.
Hercher, M., Wyntjes, G., & Deweerd, H. (1987). Non-contact laser extensometer. https://doi.org/10.1117/12.939780.
Hua, G., Yang, M., Fei, W., Lu, F., 2020. Poisson's ratios of molded pulp materials by digital image correlation method and uniaxial tensile test. J. Eng. Fibers Fabr. 15. https://doi.org/10.1177/1558925020908271.
Hunter, J.D., 2007. Matplotlib a 2d graphics environment. Comput. Sci. & Eng. 90–95.
Iliopoulos, A.P., Andrianopoulos, N.P., 2010. An Approach to Analyse Errors Introduced in the Random Grid Strain Measurement Method. Strain 46 (3), 258–266. https://doi.org/10.1111/j.1475-1305.2008.00444.x.
JCGM. (2008). Evaluation of measurement data-Guide to the expression of uncertainty in measurement Évaluation des données de mesure-Guide pour l'expression de l'incertitude de mesure. ⟨www.bipm.org⟩.
JCGM. (2012). International vocabulary of metrology-Basic and general concepts and associated terms (VIM) 3rd edition 2008 version with minor corrections Vocabulaire international de métrologie-Concepts fondamentaux et généraux et termes associés (VIM) 3 e édition.
Jeannin, T., Arnold, G., Bourmaud, A., Corn, S., De Luycker, E., Dumont, P.J.J., Ferreira, M., François, C., Grégoire, M., Harzallah, O., Heurtel, J., Joannès, S., Kervoelen, A., Labanieh, A.R., Le Moigne, N., Martoïa, F., Orgéas, L., Ouagne, P., Soulat, D., Placet, V., 2024. A round-robin study on the tensile characterization of single fibres: A multifactorial analysis and recommendations for more reliable results. Composites Part A Applied Science Manufacturing 185. https://doi.org/10.1016/j.compositesa.2024.108323.
Kahn, F., Granville, J.J. De, 1992. Palms in forest ecosystems of Amazonia. Ecol. Stud. 95.
Khoo, S.W., Karuppanan, S., Tan, C.S., 2016. A review of surface deformation and strain measurement using two-dimensional digital image correlation. In: Metrology and Measurement Systems, 23. Polish ACAD Sciences Committee Metrology and Res Equipment, pp. 461–480. https://doi.org/10.1515/mms-2016-0028.
Kissling, W.D., Baker, W.J., Balslev, H., Barfod, A.S., Borchsenius, F., Dransfield, J., Govaerts, R., Svenning, J.C., 2012. Quaternary and pre-Quaternary historical legacies in the global distribution of a major tropical plant lineage. Glob. Ecol. Biogeogr. 21 (9), 909–921. https://doi.org/10.1111/j.1466-8238.2011.00728.x.
Leclerc, H., Périé, J.-N., Besnard, G., Hild, F., Réthoré, J., Roux, S., 2010. La corrélation d'images: un outil de mécanique expérimentale. Première partie: Principes généraux. Essais & Simulations. Num 108, 2011. ⟨https://www.researchgate.net/publication/259005782⟩.
Lecompte, D., Smits, A., Bossuyt, S., Sol, H., Vantomme, J., Van Hemelrijck, D., Habraken, A.M., 2006. Quality assessment of speckle patterns for digital image correlation. Opt. Lasers Eng. 44 (11), 1132–1145. https://doi.org/10.1016/j.optlaseng.2005.10.004.
LePage, W.S., Shaw, J.A., Daly, S.H., 2017. Optimum Paint Sequence for Speckle Patterns in Digital Image Correlation. Exp. Tech. 41 (5), 557–563. https://doi.org/10.1007/s40799-017-0192-3.
Levis, C., Costa, † F.R.C., Bongers, F., Peña-Claros, M., Clement, C.R., Junqueira, A.B., Neves, E.G., Tamanaha, E.K., Figueiredo, F.O.G., Salomão, R.P., Castilho, C.V., Magnusson, W.E., Phillips, O.L., Guevara, J.E., Sabatier, D., Molino, J.-F., Cárdenas López, D., Mendoza, A.M., Pitman, N.C.A., … Ter Steege, H. (2017). Persistent effects of pre-Columbian plant domestication on Amazonian forest composition. https://doi.org/10.1126/science.aal0157.
Li, X., Fang, G., Zhao, J., Zhang, Z., Sun, L., Wang, H., Wu, X., 2021. Random Error in Strain Calculation using Regularized Polynomial Smoothing (RPS) and Point-wise Least Squares (PLS) in Digital Image Correlation. Opt. Lasers Eng. 142. https://doi.org/10.1016/j.optlaseng.2021.106590.
Li, H., Shen, S., 2011. The mechanical properties of bamboo and vascular bundles. J. Mater. Res. 26 (21), 2749–2756. https://doi.org/10.1557/jmr.2011.314.
Li, H., Zhu, Q., Lu, P., Chen, X., Xian, Y., 2024. The Gradient Variation of Location Distribution, Cross-Section Area, and Mechanical Properties of Moso Bamboo Vascular Bundles along the Radial Direction. Forests 15 (6). https://doi.org/10.3390/f15061023.
Lin, A.C., Pirrung, F., Niestrawska, J.A., Ondruschka, B., Pinter, G., Henyš, P., Hammer, N., 2024. Shape or size matters? Towards standard reporting of tensile testing parameters for human soft tissues: systematic review and finite element analysis. In: Frontiers in Bioengineering and Biotechnology, 12. Frontiers Media SA. https://doi.org/10.3389/fbioe.2024.1368383.
Liu, C., Li, S., Wang, X., Xue, Z., Shang, L., Yang, S., 2025. The bending mechanism of bamboo based on X-ray micro-tomography (μCT) and digital image correlation technique (DIC. Ind. Crops Prod. 230. https://doi.org/10.1016/j.indcrop.2025.121086.
Lu, H., Lian, H., Xu, J., Ma, N., Zhou, Z., Song, Y., Yu, Y., Zhang, X., 2022. Study on the Variation Pattern and Influencing Factors of Poisson's Ratio of Bamboo. Front. Mater. 9. https://doi.org/10.3389/fmats.2022.896756.
Lucas, B.D., Kanade, T., 1981. An Iterative Image Registration Technique with an Application to Stereo Vision. Proc. 7th Int. Jt. Conf. Artif. Intell. 674–679.
Macía, M.J., Armesilla, P.J., Cámara-Leret, R., Paniagua-Zambrana, N., Villalba, S., Balslev, H., Pardo-de-Santayana, M., 2011. Palm Uses in Northwestern South America: A Quantitative Review. Bot. Rev. 77 (Number 4), 462–570. https://doi.org/10.1007/s12229-011-9086-8.
Malowany, K., Piekarczuk, A., Malesa, M., Kujawińska, M., Wiech, P., 2019. Application of 3D digital image correlation for development and validation of FEM model of self-supporting arch structures. Appl. Sci. (Switz.) 9 (7). https://doi.org/10.3390/app9071305.
Miyoshi, Y., Kojiro, K., Furuta, Y., 2018. Effects of density and anatomical feature on mechanical properties of various wood species in lateral tension. J. Wood Sci. 64 (5), 509–514. https://doi.org/10.1007/s10086-018-1730-z.
Montúfar, R., Laffargue, A., Pintaud, J.C., Hamon, S., Avallone, S., Dussert, S., 2010. Oenocarpus bataua Mart. (arecaceae): Rediscovering a source of high oleic vegetable oil from amazonia. JAOCS. J. Am. Oil Chem. ' Soc. 87 (2), 167–172. https://doi.org/10.1007/s11746-009-1490-4.
Motra, H.B., Hildebrand, J., Dimmig-Osburg, A., 2014. Assessment of strain measurement techniques to characterise mechanical properties of structural steel. Eng. Sci. Technol. Int. J. 17 (4), 260–269. https://doi.org/10.1016/j.jestch.2014.07.006.
Muscarella, R., Emilio, T., Phillips, O.L., Lewis, S.L., Slik, F., Baker, W.J., Couvreur, T.L. P., Eiserhardt, W.L., Svenning, J.C., Affum-Baffoe, K., Aiba, S.I., de Almeida, E.C., de Almeida, S.S., de Oliveira, E.A., Álvarez-Dávila, E., Alves, L.F., Alvez-Valles, C.M., Carvalho, F.A., Guarin, F.A., Balslev, H., 2020. The global abundance of tree palms. Glob. Ecol. Biogeogr. 29 (9), 1495–1514. https://doi.org/10.1111/geb.13123.
Müssig, Jörg., 2010. Industrial Applications of Natural Fibres: Structure, Properties and Technical Applications. Wiley. https://doi.org/10.1002/9780470660324.
Mylo, M.D., Poppinga, S., 2023. Digital image correlation techniques for motion analysis and biomechanical characterization of plants (Frontiers Media SA). Front. Plant Sci. 14. https://doi.org/10.3389/fpls.2023.1335445.
Nelson, N., Stubbs, C.J., Larson, R., Cook, D.D., 2019. Measurement accuracy and uncertainty in plant biomechanics. In: Journal of Experimental Botany, 70. Oxford University Press, pp. 3649–3658. https://doi.org/10.1093/jxb/erz279.
Niklas, K.J., Spatz, H.C., 2010. Worldwide correlations of mechanical properties and green wood density. Am. J. Bot. 97 (10), 1587–1594. https://doi.org/10.3732/ajb.1000150.
Passieux, J.-Charles, Perie, J.-Noel, 2020. Advances in Digital Image Correlation (DIC. MDPI - Multidiscip. Digit. Publ. Inst. https://doi.org/10.3390/books978-3-03928-515-0.
Pickering, K.L., Efendy, M.G.A., Le, T.M., 2016. A Review of Recent Developments in Natural Fibre Composites and Their Mechanical Performance. Compos. A: Appl. Sci. Manuf. 83, 98–112. https://doi.org/10.1016/j.compositesa.2015.08.038.
Sánchez-Arévalo, F.M., Pulos, G., 2008. Use of digital image correlation to determine the mechanical behavior of materials. Mater. Charact. 59 (11), 1572–1579. https://doi.org/10.1016/j.matchar.2008.02.002.
Schneider, C.A., Rasband, W.S., Eliceiri, K.W., 2012. NIH Image to ImageJ: 25 years of image analysis. Nat. Methods 9 (Number 7), 671–675. https://doi.org/10.1038/nmeth.2089.
Seon, G., Makeev, A., Schaefer, J.D., Justusson, B., 2019. Measurement of interlaminar tensile strength and elastic properties of composites using open-hole compression testing and digital image correlation. Appl. Sci. (Switz.) 9 (13). https://doi.org/10.3390/app9132647.
Shah, J., & Harle, S.M. (2017). Saudi Journal of Civil Engineering Use of Strain Gauge in Concrete Structure. https://doi.org/10.36348/sjce.
Siddiqui, V.U., Sapuan, S.M., Isah, A., Yusuf, J., Khan, A., 2024. Advancements in multiscale oil palm fiber composites: Manufacturing techniques, performance evaluation, and industrial applications. In: Industrial Crops and Products, 213. Elsevier B.V. https://doi.org/10.1016/j.indcrop.2024.118399.
Smith, R.J., 2009. Use and misuse of the reduced major axis for line-fitting. Am. J. Phys. Anthropol. 140 (Number 3), 476–486. https://doi.org/10.1002/ajpa.21090.
Sosnowska, J., Balslev, H., 2009. American palm ethnomedicine: a meta-analysis. J. Ethnobiol. Ethnomed. 5. https://doi.org/10.1186/1746-4269-5-43.
Su, Y., Gao, Z., Zhang, Q., Wu, S., 2018. Spatial uncertainty of measurement errors in digital image correlation. Opt. Lasers Eng. 110, 113–121. https://doi.org/10.1016/j.optlaseng.2018.05.016.
Sun, F., Li, R., Zhu, J., Peng, H., Li, Z., Jiang, J., Zhan, T., Cai, L., Lyu, J., 2024. Comparison analysis of moisture-dependent orthotropic elasticity between earlywood and latewood in Chinese fir using digital image correlation. Ind. Crops Prod. 220. https://doi.org/10.1016/j.indcrop.2024.119185.
Szalai, S., Fehér, V., Kurhan, D., Németh, A., Sysyn, M., Fischer, S., 2023. Optimization of surface cleaning and painting methods for DIC measurements on automotive and railway aluminum materials. Infrastructures 8 (2). https://doi.org/10.3390/infrastructures8020027.
Taylor, B.N., & Kuyatt, C.E. (1994). Guidelines for Evaluating and Expressing the Uncertainty of NIST Measurement Results.
Ter Steege, H., Pitman, N.C.A., Sabatier, D., Baraloto, C., Salomão, R.P., Guevara, J.E., Phillips, O.L., Castilho, C.V., Magnusson, W.E., Molino, J.F., Monteagudo, A., Vargas, P.N., Montero, J.C., Feldpausch, T.R., Coronado, E.N.H., Killeen, T.J.,

Mostacedo, B., Vasquez, R., Assis, R.L., Silman, M.R., 2013. Hyperdominance in the Amazonian tree flora. Science 342 (6156). https://doi.org/10.1126/science.1243092.

Tomczak, F., Sydenstricker, T.H.D., Satyanarayana, K.G., 2007. Studies on lignocellulosic fibers of Brazil. Part II: Morphology and properties of Brazilian coconut fibers. Compos Part A Appl Sci Manuf 38, 1710–1721. https://doi.org/10.1016/j.compositesa.2007.02.004.

Trujillo, W., Rivera-Rondón, C.A., Balslev, H., 2021. Palm functional traits, soil fertility and hydrology relationships in Western Amazonia. Front. For. Glob. Change 4. https://doi.org/10.3389/ffgc.2021.723553.

Virtanen, P., Gommers, R., Oliphant, T.E., Haberland, M., Reddy, T., Cournapeau, D., Burovski, E., Peterson, P., Weckesser, W., Bright, J., van der Walt, S.J., Brett, M., Wilson, J., Millman, K.J., Mayorov, N., Nelson, A.R.J., Jones, E., Kern, R., Larson, E., Vázquez-Baeza, Y., 2020. SciPy 1.0: fundamental algorithms for scientific computing in Python. Nat. Methods 17 (3), 261–272. https://doi.org/10.1038/s41592-019-0686-2.

Yang, R., Li, Y., Zeng, D., & Guo, P. (2022). Deep DIC: Deep Learning-Based Digital Image Correlation for End-to-End Displacement and Strain Measurement.

Yu, L., Lubineau, G., 2019. Modeling of systematic errors in stereo-digital image correlation due to camera self-heating. Sci. Rep. 9 (1). https://doi.org/10.1038/s41598-019-43019-7.

Zhai, S., Imai, T., Horikawa, Y., Sugiyama, J., 2013. Anatomical and mechanical characteristics of leaf-sheath fibrovascular bundles in palms. IAWA J. 34 (3), 285–300. https://doi.org/10.1163/22941932-00000024.

Zhu, J., Tan, Y., Chen, K., Peng, H., Li, Z., Jiang, J., Lyu, J., Zhan, T., 2024. Evaluation of transverse shrinking and swelling of bamboo using digital image correlation technique. Ind. Crops Prod. 211. https://doi.org/10.1016/j.indcrop.2024.118274.